Investigations of the superconducting ground state of Zr3Ir: introducing a new noncentrosymmetric superconductor

K. P. Sajilesh, D. Singh, P. K. Biswas, Gavin B. G. Stenning, A. D. Hillier and R. P. Singh

Published version information

Citation: KP Sajilesh et al. "Investigations of the superconducting ground state of Zr3Ir: introducing a new noncentrosymmetric superconductor." Physical Review Materials, vol. 3, no. 10 (2019): 104802.

DOI: 10.1103/PhysRevMaterials.3.104802

Investigations of the superconducting ground state of Zr_3Ir: Introducing a new noncentrosymmetric superconductor

Sajilesh K. P.,[1] D. Singh,[1] P. K. Biswas,[2] Gavin B. G. Stenning,[2] A. D. Hillier,[2] and R. P. Singh[1,*]

[1]*Department of Physics, Indian Institute of Science Education and Research Bhopal, Bhopal, 462066, India*

[2]*ISIS Facility, STFC Rutherford Appleton Laboratory, Harwell Science and Innovation Campus, Oxfordshire, OX11 0QX, United Kingdom*

(Received 20 December 2018; revised manuscript received 9 August 2019; published 7 October 2019)

Superconductivity in materials whose crystal structure lacks inversion symmetry is a prime candidate for unconventional superconductivity. A new noncentrosymmetric compound Zr_3Ir crystallizes in a tetragonal α-V_3S structure. The magnetization, specific heat, and muon spin rotation confirm s-wave superconductivity, having a transition temperature $T_c = 2.3$ K. Muon spin relaxation confirms the preservation of time reversal symmetry in the superconducting ground state.

DOI: 10.1103/PhysRevMaterials.3.104802

I. INTRODUCTION

Noncentrosymmetric superconductors have attracted considerable attention recently in both theoretical and experimental condensed matter physics. The lack of inversion symmetry in these materials allow an antisymmetric spin-orbit coupling (ASOC) which can lift the degeneracy of the conduction band electrons and cause the superconducting Cooper pairs to contain an admixture of spin-singlet and spin-triplet states [1–7]. This mixed pairing may lead to superconductors with exotic properties, which are generally not observed in conventional superconductors, e.g., high upper critical field, time reversal symmetry breaking (TRSB), topologically protected edge states, and anisotropic superconducting gap [8–11]. Time reversal symmetry breaking is a rarely observed phenomenon and has only been observed in a very few unconventional superconductors [12–20]. Noncentrosymmetric materials are prime members to host TRS breaking due to admixed ground state and its mixing ratio tunability using the strength of ASOC. Several noncentrosymmetric materials have been investigated to search unconventional superconductivity, among which $LaNiC_2$ [21], La_7Ir_3 [22], Re_6X (X = Zr, Hf, Ti) [23–25], $Re_{24}Ti_5$ [26], locally noncentrosymmetric SrPtAs [27] are reported to show the presence of spontaneous static or quasistatic magnetic fields below the superconducting transition indicating a broken time reversal symmetry in the superconducting state. At the same time, many NCS superconductors are reported to show a conventional superconducting ground state [28–36]. Hence, it is important to understand the role of ASOC and electron correlations on the parity mixing in these materials to clearly understand the presence/absence of TRSB. Only a small number of noncentrosymmetric superconductors which exhibit TRSB makes it difficult to determine the roles of ASOC. Therefore it is crucial to discover and characterize new superconductors whose crystal structure lacks inversion symmetry.

In this paper, we study superconducting properties of Zr_3Ir containing heavy ($4d$ and $5d$) elements which crystallize into noncentrosymmetric tetragonal α-V_3S structure [37]. To the best of our knowledge, no other noncentrosymmetric superconductor with α-V_3S structure has been studied in detail. The noncentrosymmetric crystal structure along with the presence of heavy transition metals makes Zr_3Ir an interesting candidate to investigate the superconducting ground state. Detailed magnetization, heat capacity, and muon measurements suggest an s-wave superconducting ground state with preserved time reversal symmetry.

II. EXPERIMENTAL DETAILS

A polycrystalline sample of Zr_3Ir was prepared by conventional arc melting technique in which the constituent elements (Re powder 99.99% *Alfa Aesar*; Zr slug 99.99% *Alfa Aesar*) were taken in the stoichiometric ratio and melted in a water-cooled copper hearth under high purity argon gas. The elements were melted to form a small ash colored button of Zr_3Ir, which was flipped and remelted several times for homogeneity of the sample.

Characterization of the crystal structure and phase purity of the sample was done by room temperature x-ray diffraction measurements using PANalytical diffractometer equipped with CuK_α radiation ($\lambda = 1.5406$ Å). Magnetization and AC susceptibility measurements were done using Quantum Design superconducting quantum interference device (MPMS 3, Quantum Design). Specific heat and resistivity measurements of the sample were done in zero field as well as applied field (resistivity) using Quantum Design physical property measurement system (PPMS, Quantum Design, Inc.). The μSR experiments were carried out using 100% spin-polarized pulse muon beam at the ISIS facility, STFC Rutherford Appleton Laboratory, Didcot, United Kingdom. Both longitudinal and transverse field measurements were carried out with detectors which can be aligned accordingly while the sample was mounted on a high purity silver holder. Correction coils were used to neutralize the stray fields at the sample position.

*rpsingh@iiserb.ac.in

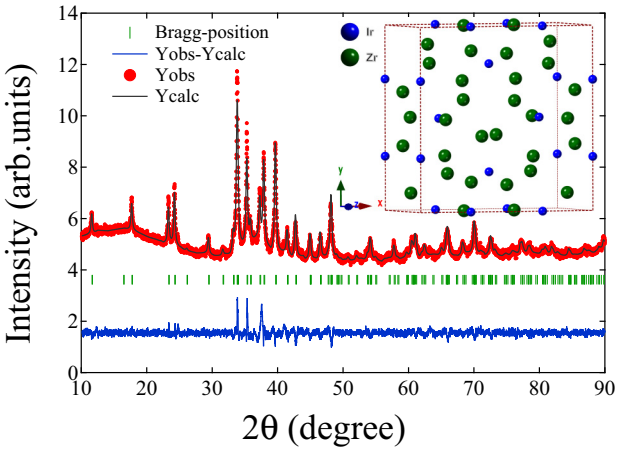

FIG. 1. Powder XRD pattern of the sample recorded at ambient temperature using CuK_α radiation (red line). The Rietveld refined data for the noncentrosymmetric space group I-42m (121) is shown as a dotted black line. The green vertical lines show the calculated reflection positions. The inset displays a unit cell of Zr_3Ir.

III. RESULTS AND DISCUSSIONS

A. Crystallography

Figure 1 shows the x-ray diffraction pattern of Zr_3Ir. The structural refinement of the data was carried out using Fullprof software. It confirms that the sample crystallized in the noncentrosymmetric tetragonal α-V_3S structure (space group no. 121) with no impurity. The lattice parameters obtained from refinement are $a = b = 10.788(4)$ Å, $c = 5.602(2)$ Å, consistent with earlier reports [37]. Noncentrosymmetric nature of crystal structure can be seen from the arrangement of Zr atoms (Fig. 1 inset). A detailed description regarding the crystal structure can be seen in Ref. [37].

B. Resistivity

Figure 2 shows the resistivity of Zr_3Ir as a function of temperature. The transition temperature, observed from the resistivity measurement, was around $T_c^{\text{onset}} = 2.32 \pm 0.03$ K. The low temperature ($T_c < T \ll \theta_D$,) resistivity data show power law behavior where θ_D is the Debye temperature determined from specific heat measurement. The inset shows an expanded plot of resistivity around the transition temperature. Low temperature resistivity data in the range 5 K $\leqslant T \leqslant$ 45 K can be fitted fairly well with the equation

$$\rho(T) = \rho_0 + AT^n. \tag{1}$$

Here ρ_0 is the residual resistivity due to crystallographic defects and disorders while the second term adds the electronic contribution to resistivity due to electron-electron correlation. Fitting with $n = 2.1$ yields the values as $\rho_0 = (64.9 \pm 0.1) \times 10^{-6}$ Ω cm and $A = (0.047 \pm 0.006) \times 10^{-6}$ Ω cm K^{-2}. A deviation from ideal Fermi behavior can be attributed to increased scattering in the system.

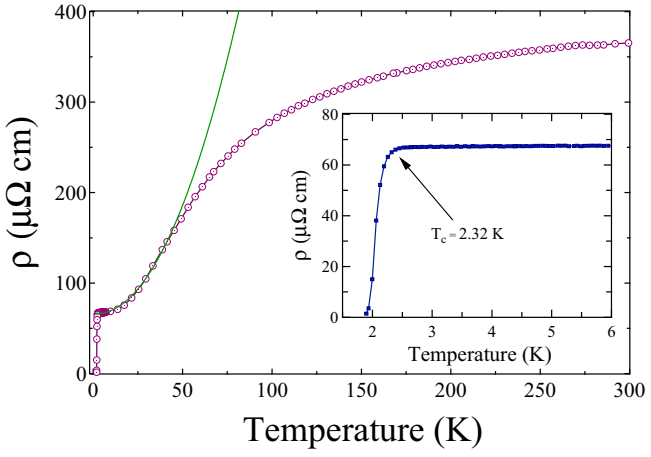

FIG. 2. Resistivity measurement taken against temperature $\rho(T)$ at zero field. The inset shows the drop in resistivity at $T_c = 2.3$ K. The green line is a fit to low temperature data using power law.

C. Magnetization

The DC magnetic susceptibility measured in both zero field cooled (ZFC) and field cooled cooling (FCC) mode in an applied field of 10 Oe also confirms the bulk superconductivity with transition temperature $T_c^{\text{onset}} = 2.33 \pm 0.05$ K [Fig. 3(a)]. A superconducting fraction exceeding 100% is accounted for by the uncorrected geometrical factor. Figure 3(b) depicts the low field magnetization data taken at different temperatures. The magnetization increases linearly with applied field after which it deviates due to vortex formation. The point of deviation from linear behavior of the data is taken as the H_{c1} at each temperature. $H_{c1}(T)$ is modeled using the Ginzburg-Landau relation $H_{c1}(T) = H_{c1}(0)(1 - t^2)$, where $t = T/T_c$, and we found $H_{c1}(0) = 66 \pm 4$ Oe.

The upper critical field was estimated by magnetization as well as resistivity measurements at the different applied field in the range 100 Oe $\leqslant$ H $\leqslant$ 3 kOe. The value of H_{c2} at each field is taken as the 90% of the fall in moment/resistivity. It was seen from both the measurements that the T_c shifted towards lower value with a broader transition as field increased [Fig. 3(d) inset]. Magnetization data collected against the applied field at different temperatures down to 0.4 K is shown in Fig. 3(c). It is visible from the figure that the area of hysteresis loop decreases as the temperature is increased towards T_c, characteristic of type-II superconductor. A discontinuity in slope at a field, as shown in inset [Fig. 3(c)] is identified as H_{c2} at each temperature. The value of $H_{c2}(0)$ is determined by fitting $H_{c2}(T)$ using the relation

$$H_{c2}(T) = H_{c2}(0)\frac{(1 - t^2)}{(1 + t^2)}, \tag{2}$$

where $t = T/T_c$ is the reduced temperature. Fitting the magnetization data using the equation yields $H_{c2}(0) = 9.68 \pm 0.42$ kOe. The value of $H_{c2}(0)$ can be used to find Ginzburg-Landau coherence length using the equation $\xi_{GL} = (\phi_0/2\pi H_{c2}(0))^{1/2}$, where ϕ_0 is the flux quantum($\phi_0 = 2.07 \times 10^{-15}$ Tm^2). Substituting the value of $H_{c2}(0)$ gives $\xi_{GL} = 185 \pm 4$ Å. Magnetic penetration depth for the sample $\lambda_{GL}(0)$ is estimated using the relation

$$H_{c1}(0) = \frac{\Phi_0}{4\pi\lambda_{GL}^2(0)}\left(\ln\frac{\lambda_{GL}(0)}{\xi_{GL}(0)} + 0.12\right) \tag{3}$$

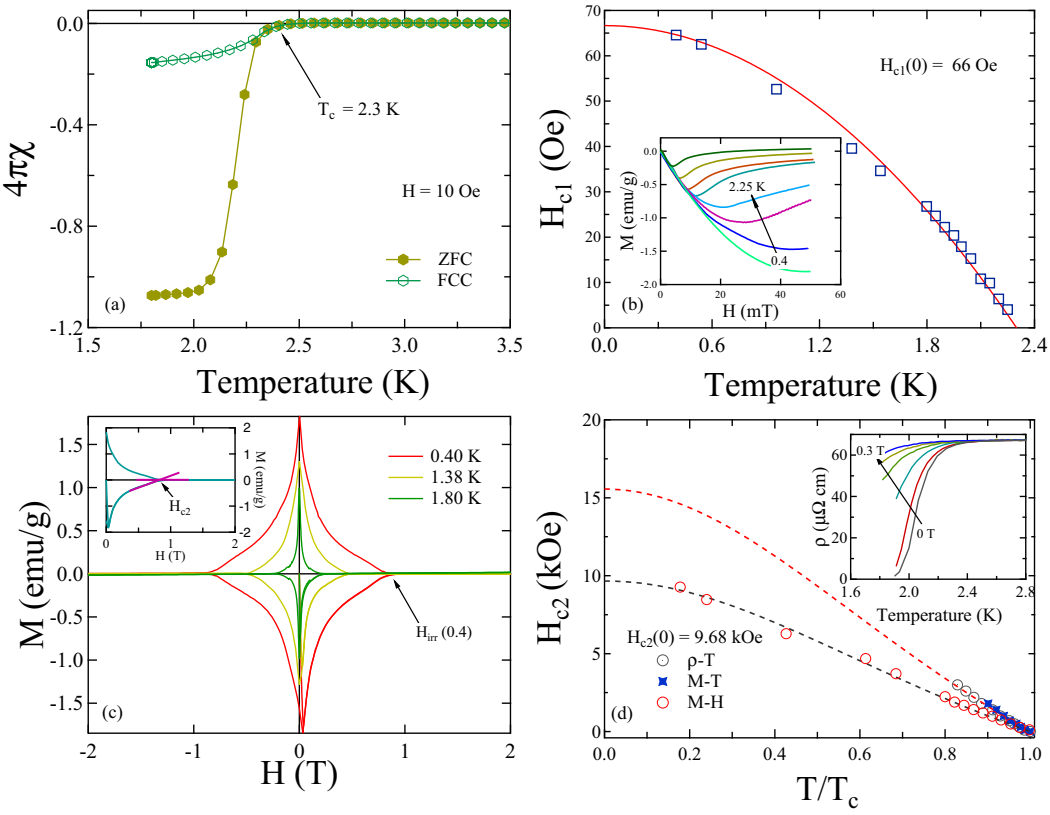

FIG. 3. (a) Temperature dependence of magnetic susceptibility collected via both ZFC and FCC mode. Superconducting transition of the sample is observed at $T_c = 2.3$ K. (b) Temperature variation of lower critical field H_{c1} collected via magnetization measurement. Extrapolation using G-L equation gives $H_{c1}(0) = 66$ Oe. The inset shows the magnetization curves taken up to 500 Oe at different temperatures. (c) Isothermal magnetization curve taken at different temperatures. The inset shows the enlarged view. H_{c2} is taken at the discontinuity in the gradient as marked in the inset. (d) Determination of upper critical field $H_{c2}(0)$ using magnetization and resistivity measurements. The dotted lines indicates the fits to the data using Eq. (2). The inset shows low temperature resistivity data collected at different fields.

which is obtained as 2624 ± 68 Å. This can be used to estimate Ginzburg-Landau parameter $k = \lambda_{GL}(0)/\xi_{GL}(0) = 14.2 \pm 0.8$, indicating the type II nature of the sample.

One of the mechanisms which causes the breaking of Cooper pair is the Pauli limiting field effect, in which the applied magnetic field induces the spin to align in the same direction of the magnetic field. The Pauli limiting field is estimated as $H^p_{c2}(0) = 1.86T_c = 42.8 \pm 0.6$ kOe. This is larger than the $H_{c2}(0)$ obtained from magnetization as well as resistivity measurements. Another pair breaking mechanism is the orbital limiting field effect, $H^{\text{orbital}}_{c2}(0)$, which can be calculated by Werthermar-Helfand-Hohenberg expression [38,39],

$$H^{\text{orbital}}_{c2}(0) = -\alpha T_c \left.\frac{dH_{c2}(T)}{dT}\right|_{T=T_c} \quad (4)$$

according to which the kinetic energy of the superelectron exceeds the condensation energy causing the Cooper pair breaking. Substituting $\alpha = 0.693$ for dirty limit superconductors (Dirty limit nature for Zr_3Ir is shown in the last section) and initial slope at $T = T_c$, $\frac{-dH_{c2}(T)}{dT} = 4.96 \pm 0.11$ kOe/K gives $H^{\text{orbital}}_{c2}(0) \approx 7.75 \pm 0.03$ kOe. The values of $H^p_{c2}(0)$ and $H^{\text{orbital}}_{c2}(0)$ suggest that the orbital limiting field effect is the dominant pair breaking mechanism. A small value of the Maki parameter, $\alpha_M = \sqrt{2}H^{orb}_{c2}(0)/H^p_{c2}(0) = 0.26 \pm 0.01$ also indicates a negligible effect of Pauli limiting field.

D. Specific heat

Heat capacity measurements with temperature confirm the superconducting transition at $T_c = 2.31 \pm 0.05$ K. Transition temperature is consistent with the magnetization and resistivity data. Specific heat data was taken in the range 1 K $\leqslant T \leqslant$ 15 K and normal state specific data was fitted using the relation $C/T = \gamma_n + \beta T^2$ which allows the determination of the electronic contribution to specific heat $\gamma_n = 16.52 \pm 0.09$ mJ/mol K^2 and the phononic contribution, $\beta = 0.618 \pm 0.001$ mJ/mol K^4 (see Fig. 4).

The electronic contribution to specific heat is calculated by subtracting the phononic contribution from the total specific heat ($C_{el} = C - \beta T^3$). The normalized jump in specific heat $\frac{\Delta C_{el}}{\gamma_n T_c}$ came out to be 0.97 ± 0.05 which is less than the BCS value of $\frac{\Delta C_{el}}{\gamma_n T_c} = 1.43$ in the weak coupling limit. A similar low value of specific heat jump is reported for many other noncentrosymmetric materials [31,40]. This can be attributed to inhomogeneity in the sample or due to the presence of regions which do not participate in superconductivity.

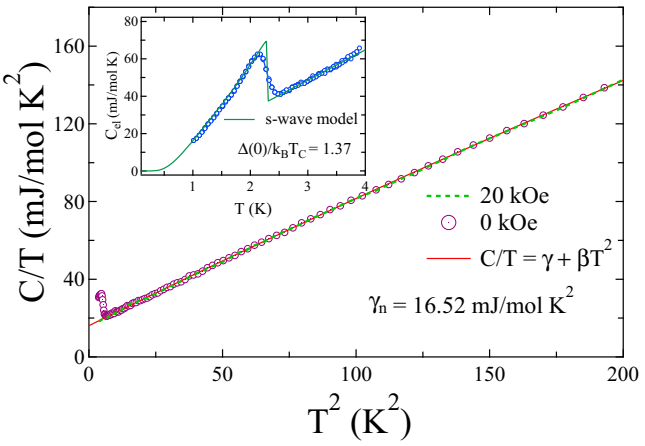

FIG. 4. C/T Vs T^2 shows a jump in specific heat at 2.31 K. An applied field of 20 kOe (green dotted line) which is above $H_{C2}(0)$ kills the superconducting transition. (Inset) Variation of electronic specific heat with temperature is fitted by the isotropic s-wave model (green line). The fitting yields the value of superconducting gap as $\frac{\Delta(0)}{k_B T_c} = 1.37$.

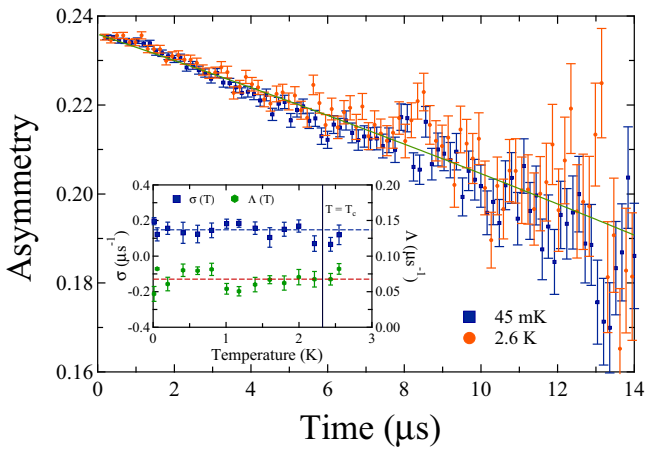

FIG. 5. μSR spectra collected in zero field configuration at temperatures above (2.6 K) and below (45 mK) the transition temperature. The inset shows no significant change in fit parameters $\Lambda(T)$ and $\sigma(T)$ across the transition temperature.

Debye temperature of the sample θ_D can be calculated using the value of β with the equation $\theta_D = (12\pi^4 RN/5\beta)^{\frac{1}{3}}$. Substituting the value of R, the universal gas constant, and number of atoms per formula unit cell N = 4 gives $\theta_D = 232 \pm 8$ K. Electronic density of states at the Fermi level $D_C(E_f)$ is proportional to the Sommerfeld coefficient γ_n. This can be calculated using the relation $\gamma_n = (\pi^2 k_B^2/3) D_C(E_f)$, which gives $D_C(E_f) = 7.01 \pm 0.03 \ \frac{states}{eV f.u}$. Once the Debye temperature θ_D is determined, one can use McMillans Eq. (5) [41] to evaluate the electron phonon coupling constant, a dimensionless number which says about the relative strength of electron-phonon coupling

$$\lambda_{e\text{-}ph} = \frac{1.04 + \mu^* \ln(\theta_D/1.45T_c)}{(1 - 0.62\mu^*)\ln(\theta_D/1.45T_c) - 1.04}. \quad (5)$$

This provides us $\lambda_{e\text{-}ph} = 0.56 \pm 0.04$ indicating Zr_3Ir is an intermediately coupled superconductor. The bare-band structure density of states $D_{\text{band}}(E_f)$ is related to electron-phonon coupling strength $\lambda_{e\text{-}ph}$ and can be calculated using $D_C(E_f) = D_{\text{band}}(E_f)(1 + \lambda_{e\text{-}ph})$ which gives $D_{\text{band}}(E_f) = 4.5 \pm 0.3 \ \frac{states}{eV f.u}$. The effective mass m^* of the quasiparticle came out to be $1.56 m_e$ using the relation $m^* = m^*_{\text{band}}(1 + \lambda_{e\text{-}ph})$, where we have used $m^*_{\text{band}} = m_e$.

The behavior of electronic specific heat gives salient features of superconducting gap structure. The temperature dependence of electronic specific heat C_{el} is shown in Fig. 4. The superconducting contribution to entropy (S) as described by BCS theory is

$$\frac{S}{\gamma_n T_c} = -\frac{6}{\pi^2}\left(\frac{\Delta(0)}{k_B T_c}\right)\int_0^\infty [f\ln(f) + (1-f)\ln(1-f)]dy \quad (6)$$

where the integral is taken over the energies of normal electrons relative to the Fermi level. $f(\xi) = [\exp(E(\xi)/k_B T)+1]^{-1}$ is the Fermi-Dirac distribution function. The energy of the quasiparticle is given by $E(\xi) = \sqrt{\xi^2 + \Delta^2(t)}$, where $y = \xi/\Delta(0)$, $t = T/T_c$, and $\Delta(t) = \tanh[1.82(1.018((I/t)\text{-}1))^{0.51}]$ is the BCS approximation for the temperature dependence of the energy gap. The normalized electronic specific heat can be related to normalized entropy by

$$\frac{C_{el}}{\gamma_n T_c} = t\frac{d(S/\gamma_n T_c)}{dt} \quad (7)$$

where C_{el} below T_c is described by the above equation whereas above T_c it's equal to $\gamma_n T_c$. The data was fitted quite well with the equation (7). This yielded the value of the superconducting energy gap as $\frac{\Delta(0)}{k_B T_c} = 1.37 \pm 0.04$. The value obtained is below the BCS predicted value $\frac{\Delta(0)}{k_B T_c} = 1.76$.

E. Muon spin relaxation and rotation

A further investigation of the superconducting ground state was undertaken by muon spin relaxation and rotation measurements. Zero field muon spin relaxation spectra were collected at different temperatures above and below the T_c. Figure 5 shows the representative spectra at 2.6 K and 45 mK. The absence of any oscillatory component in the data rules out the presence of any spontaneous coherent field associated with the ordered magnetic structure. In the absence of any coherent magnetic ordering, muon spin relaxation is determined primarily by randomly oriented local nuclear dipole moments, which can be modeled by the Gaussian Kubo-Toyabe (KT) function

$$G_{\text{KT}}(t) = \frac{1}{3} + \frac{2}{3}(1 - \sigma_{\text{ZF}}^2 t^2)\exp\left(\frac{-\sigma_{\text{ZF}}^2 t^2}{2}\right) \quad (8)$$

where σ_{ZF} corresponds to the relaxation due to static, randomly oriented local fields associated with the nuclear moments at the muon site. The zero field spectra of Zr_3Ir can be well described by the function

$$A(t) = A_1 G_{\text{KT}}(t)\exp(-\Lambda t) + A_{\text{BG}} \quad (9)$$

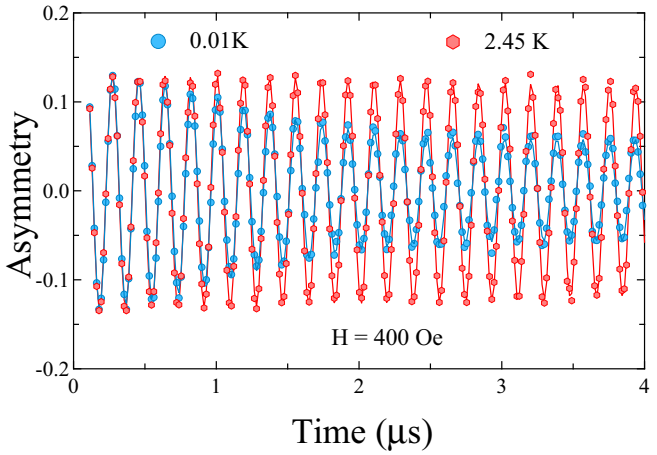

FIG. 6. A representative μSR spectra collected in transverse field configuration at an applied field of 400 Oe. The spectra collected at 0.01 K show significant decay due to flux line lattice formation, while the nondecaying nature of the signal at $T = 2.45$ K indicates uniform field distribution above T_c.

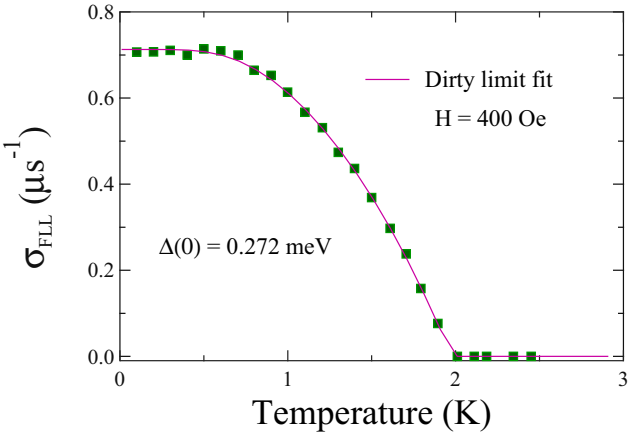

FIG. 7. Temperature dependence of σ_{FLL} measured at an applied field of 400 Oe. The solid red line is the dirty limit isotropic s-wave fit for the data.

where A_1 corresponds to the sample asymmetry, Λ is the additional electronic relaxation rate, and A_{BG} is the temperature independent background asymmetry coming from the muons stopped in the silver sample holder. Reportedly, in superconducting systems where time-reversal symmetry is broken, spontaneous magnetic moments arise below T_c, and an increase may be observed in either σ_{ZF} or Λ. Fitting Eq. (9) at different data sets above and below T_c yields similar values of σ_{ZF} and Λ with no noticeable change (see inset Fig. 5). This suggests that the time reversal symmetry is preserved in the superconducting phase.

Superconducting gap structure of Zr_3Ir was examined using transverse field μSR (TF-μSR). TF-μSR precession signal was collected at 400 Oe, which is well above the lower critical field. During the experiment, the sample was field cooled to the low temperature to ensure the formation of a well-ordered flux line lattice (FLL). Figure 6 shows the muon spin rotation spectra measured at either side of transition temperature T_c. It is quite evident from the graph that the quick decay in spectra below T_c is accounted for by the formation of FLL, which causes inhomogeneous field distribution. The TF-μSR signal is well described by the oscillatory decaying function given by

$$G_{\mathrm{TF}}(t) = A_1 \exp\left(\frac{-\sigma^2 t^2}{2}\right)\cos(w_1 t + \phi) + A_2 \cos(w_2 t + \phi), \tag{10}$$

where $\omega_1 = \gamma_\mu B_1$ and $\omega_2 = \gamma_\mu B_2$ are the muon precessional frequencies for sample and background, respectively, ϕ is the initial phase offset, σ is the total depolarization rate, and γ_μ is the muon gyromagnetic ratio. The field distribution due to FLL is broadened by the presence of randomly oriented nuclear magnetic moments. Hence the total depolarization rate σ is written as

$$\sigma^2 = \sigma_{\mathrm{N}}^2 + \sigma_{\mathrm{FLL}}^2. \tag{11}$$

Here σ_{N} corresponds to depolarization due to nuclear moments and σ_{FLL} corresponds to that from FLL.

According to the model which explains dirty limit (see next page) s-wave superconductors, the temperature dependence of μSR depolarization rate in the vortex state can be written as

$$\frac{\sigma_{FLL}(T)}{\sigma_{FLL}(0)} = \frac{\Delta(T)}{\Delta(0)}\tanh\left[\frac{\Delta(T)}{2k_BT}\right], \tag{12}$$

where $\Delta(T) = \Delta_0\delta(T/T_c)$ and $\delta(T/T_c) = \tanh[1.82(1.018((T_c/T)-1))^{0.51}]$ is the BCS approximation for temperature dependence of superconducting energy gap. Combining Eqs. (11) and (12), a model is obtained where $\sigma(T)$ below T_c is well described by the relation

$$\sigma(T) = \sqrt{\sigma_{\mathrm{FLL}}^2(0)\frac{\Delta^2(T)}{\Delta^2(0)}\tanh^2\left[\frac{\Delta(T)}{2k_BT}\right] + \sigma_{\mathrm{N}}^2} \tag{13}$$

whereas above T_c it is simply equal to σ_N. Figure 7 represents temperature dependent depolarization rate due to FLL at 400 Oe, calculated using Eq. (11). The depolarization rate $\sigma_{FLL}(T)$ is zero as expected above T_c. The best fit to the data using Eq. (12) gives $\Delta(0) = 0.272$ meV. This gives the normalized energy gap at T_c, $\frac{\Delta(0)}{k_BT_c} = 1.372$, which accurately matches with the results from specific heat measurement.

The results from the bulk measurements can be effectively used to determine more parameters for Zr_3Ir which characterizes the superconducting ground state. A set of four equations as explained in Refs. [42,43] is solved to get superconducting carrier density n, effective mass m*, BCS coherence length ξ_0, and mean free path l and are tabulated in Table I. Solving these has confirmed that the sample is in the dirty limit regime ($\xi_0 > l_e$) justifying the dirty limit model used in both specific heat and muon spectra analysis. The Fermi temperature (T_F) of the sample can be extracted from the relation

$$k_BT_F = \frac{\hbar^2}{2}(3\pi^2)^{2/3}\frac{n^{2/3}}{m^*}, \tag{14}$$

TABLE I. Normal and superconducting properties of noncentrosymmetric superconductor Zr_3Ir.

Parameter	Unit	Value
T_c	K	2.33
$H_{c1}(0)$	Oe	66
$H_{c2}(0)$	kOe	9.68
$H^P_{c2}(0)$	kOe	42.8
ξ_{GL}	Å	185
λ_{GL}	Å	2624
κ_{GL}		14.2
$\Delta C_{el}/\gamma_n T_c$		0.97
$\Delta(0)/k_B T_c$		1.37
m^*/m_e		14.8
n	10^{27} m^{-3}	13.8
l	Å	34.66
ξ_0	Å	46
ξ_0/l		1.33
v_f	10^4 ms^{-1}	5.81
λ_L	Å	1739
T_c/T_F		0.0014

which gives the effective Fermi temperature $T_F = 1645$ K. In general, high T_c superconductors and other unconventional superconductors fall in the range $0.01 \leqslant T_c/T_F \leqslant 0.1$ [44–46]. For Zr_3Ir the ratio $\frac{T_c}{T_F}$ comes around 0.0014 which places our sample away from the unconventional family as shown in Fig. 8.

At this point, it will be worth it to discuss the dirty limit nature of the sample which can have implications on the measurements determining the superconducting gap structure, as done in Ref. [49]. A superconductor in the dirty limit regime will have an increased scattering from impurities and defects. This effect can have impacts on different measurements at low temperatures, which in turn can give slightly different results, suppressing nodal or anisotropic behavior. A notable example is the case of $Mg_{10}Ir_{19}B_{16}$ where a sample with residual resistivity 1400 $\mu\Omega$ cm [50] has shown no evidence of unconventional gap structure. While a comparatively clean sample of $Mg_{10}Ir_{19}B_{16}$ with a residual resistivity value of 100 $\mu\Omega$ cm [51] has shown a two gap behavior at low temperature penetration depth study using tunnel diode oscillator. Though most of the superconductors which have shown nonisotropic behavior like $CePt_3Si$, Li_2Pt_3B falls in the clean limit regime, many noncentrosymmetric superconductors with considerable residual resistivity value has shown an isotropic s-wave behavior. Considering the present case of Zr_3Ir, the sample has shown a residual resistivity value of 61 $\mu\Omega$ cm, which is comparatively less and the depolarization rate is seen temperature independent below 0.7 K within the statistical uncertainty. This strongly suggests that the sample has an isotropic gap, and any other possibility can be ruled out.

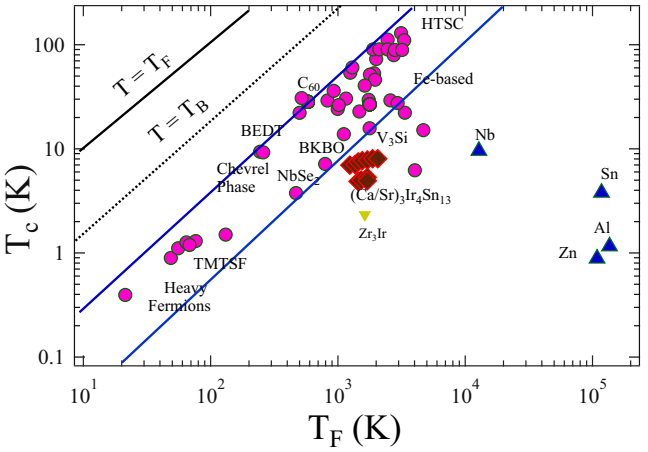

FIG. 8. The Uemura plot showing the superconducting transition temperature T_c vs the effective Fermi temperature T_F, where Zr_3Ir is shown as an inverted yellow triangle. Other data points plotted between the blue solid lines are the different families of unconventional superconductors [47,48].

IV. CONCLUSIONS

In conclusion, we have studied the superconducting properties of Zr_3Ir, which belong to the tetragonal noncentrosymmetric α-V_3S family. This is one of the first superconductors of this family. The transport, magnetization, and specific heat measurements confirm a type-II superconductivity with $T_c = 2.3$ K. The lower and upper critical field value is estimated as $H_{c1} = 66 \pm 4$ Oe and $H_{c2} = 9.68 \pm 0.42$ kOe. The characteristic length scale for the compound is estimated using the G-L relations which came out to be $\xi_{GL} = 185 \pm 4$ Å and $\lambda_{GL} = 2624 \pm 68$ Å. The value of the normalized specific heat jump $\frac{\Delta C_{el}}{\gamma T_c} = 0.97 \pm 0.05$ along with the superconducting region fitted using the weak coupling limit BCS expression suggested that Zr_3Ir is a s-wave superconductor with isotropic gap $\frac{\Delta(0)}{k_B T_c} = 1.37$. This was further confirmed by TF-μSR measurements. μSR measurements also rule out the presence of any spontaneous magnetic field arising in the superconducting state, confirming the preserved time reversal symmetry for the system in the sensitivity limit of the muon. To understand the role of the structure/pairing symmetry in noncentrosymmetric superconductors, further experimental work coupled with theoretical calculations is vital. This work paves the way for further studies on new members from the α-V_3S family of compounds to understand the role of the different crystal structure (noncentrosymmetric)/spin orbital coupling on time reversal symmetry breaking in noncentrosymmetric superconductors.

ACKNOWLEDGMENTS

R.P.S. acknowledges Science and Engineering Research Board, Government of India for the Young Scientist Grant No. YSS/2015/001799 and Financial support from DST FIST Project No. SR/FST/PSI-195/2014(C) is also thankfully acknowledged. We thank ISIS, STFC, UK for the beamtime to conduct the μSR experiments [52].

[1] E. Bauer and M. Sigrist, *Non-centrosymmetric Superconductor:Introduction and Overview* (Springer-Verlag, Heidelberg, 2012).

[2] L. P. Gor'kov and E. I. Rashba, Phys. Rev. Lett. **87**, 037004 (2001).

[3] P. A. Frigeri, D. F. Agterberg, A. Koga, and M. Sigrist, Phys. Rev. Lett. **92**, 097001 (2004).

[4] P. A. Frigeri, D. F. Agterberg, and M. Sigrist, New J. Phys. **6**, 115 (2004).

[5] V. M. Edel'shtein, Sov. Phys. JETP **68**, 1244 (1989).

[6] K. V. Samokhin, E. S. Zijlstra, and S. K. Bose, Phys. Rev. B **69**, 094514 (2004).

[7] S. Fujimoto, J. Phys. Soc. Jpn. **76**, 051008 (2007).

[8] E. Bauer, G. Hilscher, H. Michor, C. Paul, E. W. Scheidt, A. Gribanov, Y. Seropegin, H. Noël, M. Sigrist, and P. Rogl, Phys. Rev. Lett. **92**, 027003 (2004).

[9] Y. Tanaka, Y. Mizuno, T. Yokoyama, K. Yada, and M. Sato, Phys. Rev. Lett. **105**, 097002 (2010).

[10] X. L. Qi and S. C. Zhang, Rev. Mod. Phys. **83**, 1057 (2011).

[11] I. Bonalde, W. Brämer-Escamilla, and E. Bauer, Phys. Rev. Lett. **94**, 207002 (2005).

[12] G. M. Luke, Y. Fudamoto, K. M. Kojima, M. I. Larkin, J. Merrin, B. Nachumi, Y. J. Uemura, Y. Maeno, Z. Q. Mao, Y. Mori, H. Nakamura, and M. Sigrist, Nature (London) **394**, 558 (1998).

[13] J. Xia, Y. Maeno, P. T. Beyersdorf, M. M. Fejer, and A. Kapitulnik, Phys. Rev. Lett. **97**, 167002 (2006).

[14] G. M. Luke, A. Keren, L. P. Le, W. D. Wu, Y. J. Uemura, D. A. Bonn, L. Taillefer, and J. D. Garrett, Phys. Rev. Lett. **71**, 1466 (1993).

[15] R. H. Heffner, J. L. Smith, J. O. Willis, P. Birrer, C. Baines, F. N. Gygax, B. Hitti, E. Lippelt, H. R. Ott, A. Schenck, E. A. Knetsch, J. A. Mydosh, and D. E. MacLaughlin, Phys. Rev. Lett. **65**, 2816 (1990).

[16] Y. Aoki, A. Tsuchiya, T. Kanayama, S. R. Saha, H. Sugawara, H. Sato, W. Higemoto, A. Koda, K. Ohishi, K. Nishiyama, and R. Kadono, Phys. Rev. Lett. **91**, 067003 (2003).

[17] A. Maisuradze, W. Schnelle, R. Khasanov, R. Gumeniuk, M. Nicklas, H. Rosner, A. Leithe-Jasper, Y. Grin, A. Amato, and P. Thalmeier, Phys. Rev. B **82**, 024524 (2010).

[18] A. D. Hillier, J. Quintanilla, B. Mazidian, J. F. Annett, and R. Cywinski, Phys. Rev. Lett. **109**, 097001 (2012).

[19] A. Bhattacharyya, D. T. Adroja, J. Quintanilla, A. D. Hillier, N. Kase, A. M. Strydom, and J. Akimitsu, Phys. Rev. B **91**, 060503(R) (2015).

[20] T. Shang, M. Smidman, S. K. Ghosh, C. Baines, L. J. Chang, D. J. Gawryluk, J. A. T. Barker, R. P. Singh, D. McK. Paul, G. Balakrishnan, E. Pomjakushina, M. Shi, M. Medarde, A. D. Hillier, H. Q. Yuan, J. Quintanilla, J. Mesot, and T. Shiroka, Phys. Rev. Lett. **121**, 257002 (2018)

[21] A. D. Hillier, J. Quintanilla, and R. Cywinski, Phys. Rev. Lett. **102**, 117007 (2009).

[22] J. A. T. Barker, D. Singh, A. Thamizhavel, A. D. Hillier, M. R. Lees, G. Balakrishnan, D. McK. Paul, and R. P. Singh, Phys. Rev. Lett. **115**, 267001 (2015).

[23] R. P. Singh, A. D. Hillier, B. Mazidian, J. Quintanilla, J. F. Annett, D. McK. Paul, G. Balakrishnan, and M. R. Lees, Phys. Rev. Lett. **112**, 107002 (2014).

[24] D. Singh, J. A. T. Barker, A. Thamizhavel, D. McK. Paul, A. D. Hillier, and R. P. Singh, Phys. Rev. B **96**, 180501(R) (2017).

[25] D. Singh, Sajilesh K. P., J. A. T. Barker, D. M. Paul, A. D. Hillier, and R. P. Singh, Phys. Rev. B **97**, 100505(R) (2018).

[26] T. Shang, G. M. Pang, C. Baines, W. B. Jiang, W. Xie, A. Wang, M. Medarde, E. Pomjakushina, M. Shi, J. Mesot, H. Q. Yuan, and T. Shiroka, Phys. Rev. B **97**, 020502(R) (2018).

[27] P. K. Biswas, H. Luetkens, T. Neupert, T. Sturzer, C. Baines, G. Pascua, A. P. Schnyder, M. H. Fischer, J. Goryo, M. R. Lees, H. Maeter, F. Brückner, H.-H. Klauss, M. Nicklas, P. J. Baker, A. D. Hillier, M. Sigrist, A. Amato, and D. Johrendt, Phys. Rev. B **87**, 180503(R) (2013).

[28] F. Kneidinger, H. Michor, A. Sidorenko, E. Bauer, I. Zeiringer, P. Rogl, C. Blaas-Schenner, D. Reith, and R. Podloucky, Phys. Rev. B **88**, 104508 (2013).

[29] V. K. Anand, A. D. Hillier, D. T. Adroja, A. M. Strydom, H. Michor, K. A. McEwen, and B. D. Rainford, Phys. Rev. B **83**, 064522 (2011).

[30] J. A. T. Barker, B. D. Breen, R. Hanson, A. D. Hillier, M. R. Lees, G. Balakrishnan, D. McK. Paul, and R. P. Singh, Phys. Rev. B **98**, 104506 (2018).

[31] Y. Qi, J. Guo, H. Lei, Z. Xiao, T. Kamiya, and H. Hosono, Phys. Rev. B **89**, 024517 (2014).

[32] R. P. Singh, A. D. Hillier, D. Chowdhury, J. A. T. Barker, D. McK. Paul, M. R. Lees, and G. Balakrishnan, Phys. Rev. B **90**, 104504 (2014).

[33] M. Smidman, A. D. Hillier, D. T. Adroja, M. R. Lees, V. K. Anand, R. P. Singh, R. I. Smith, D. M. Paul, and G. Balakrishnan, Phys. Rev. B **89**, 094509 (2014).

[34] V. K. Anand, D. Britz, A. Bhattacharyya, D. T. Adroja, A. D. Hillier, A. M. Strydom, W. Kockelmann, B. D. Rainford, and K. A. McEwen, Phys. Rev. B **90**, 014513 (2014).

[35] W. Wei, G. J. Zhao, D. R. Kim, C. Jin, J. L. Zhang, L. Ling, L. Zhang, H. Du, T. Y. Chen, J. Zang, M. Tian, C. L. Chien, and Y. Zhang, Phys. Rev. B **94**, 104503 (2016).

[36] M. Isobe, M. Arai, and N. Shirakawa, Phys. Rev. B **93**, 054519 (2016).

[37] K. Cenzual and E. Parthé, Acta Cryst. C **41**, 820 (1985).

[38] E. Helfand and N. R. Werthamer, Phys. Rev. **147**, 288 (1966).

[39] N. R. Werthamer, E. Helfand, and P. C. Hohenberg, Phys. Rev. **147**, 295 (1966).

[40] C. B. Vining, R. N. Shelton, H. F. Braun, and M. Pelizzone, Phys. Rev. B **27**, 2800 (1983).

[41] W. L. McMillan, Phys. Rev. **167**, 331 (1968)

[42] D. A. Mayoh, J. A. T. Barker, R. P. Singh, G. Balakrishnan, D. McK. Paul, and M. R. Lees, Phys. Rev. B **96**, 064521 (2017).

[43] A. D. Hillier and R. Cywinski, Appl. Magn. Reson. **13**, 95 (1997).

[44] Y. J. Uemura, L. P. Le, G. M. Luke, B. J. Sternlieb, W. D. Wu, J. H. Brewer, T. M. Riseman, C. L. Seaman, M. B. Maple, M. Ishikawa, D. G. Hinks, J. D. Jorgensen, G. Saito, and H. Yamochi, Phys. Rev. Lett. **66**, 2665 (1991).

[45] Y. J. Uemura, V. J. Emery, A. R. Moodenbaugh, M. Suenaga, D. C. Johnston, A. J. Jacobson, J. T. Lewandowski, J. H. Brewer, R. F. Kiefl, S. R. Kreitzman, G. M. Luke, T. Riseman, C. E. Stronach, W. J. Kossler, J. R. Kempton, X. H. Yu, D. Opie, and H. E. Schone, Phys. Rev. B **38**, 909 (1988).

[46] Y. J. Uemura, G. M. Luke, B. J. Sternlieb, J. H. Brewer, J. F. Carolan, W. N. Hardy, R. Kadono, J. R. Kempton, R. F. Kiefl, S. R. Kreitzman, P. Mulhern, T. M. Riseman, D. L. Williams, B. X. Yang, S. Uchida, H. Takagi, J. Gopalakrishnan, A. W. Sleight, M. A. Subramanian, C. L. Chien, M. Z. Cieplak, G.

Xiao, V. Y. Lee, B. W. Statt, C. E. Stronach, W. J. Kossler, and X. H. Yu, Phys. Rev. Lett. **62**, 2317 (1989).

[47] K. Hashimoto, K. Cho, T. Shibauchi, S. Kasahara, Y. Mizukami, R. Katsumata, Y. Tsuruhara, T. Terashima, H. Ikeda, M. A. Tanatar, H. Kitano, N. Salovich, R. W. Giannetta, P. Walmsley, A. Carrington, R. Prozorov, and Y. Matsuda, Science **336**, 1554 (2012).

[48] R. Khasanov, H. Luetkens, A. Amato, H. H. Klauss, Z. A. Ren, J. Yang, W. Lu, and Z. X. Zhao, Phys. Rev. B **78**, 092506 (2008).

[49] B. A. Frandsen, S. C. Cheung, T. Goko, L. Liu, T. Medina, T. S. J. Munsie, G. M. Luke, P. J. Baker, Marco P. Jimenez S., G. Eguchi, S. Yonezawa, Y. Maeno, and Y. J. Uemura, Phys. Rev. B **91**, 014511 (2015).

[50] A. A. Aczel, T. J. Williams, T. Goko, J. P. Carlo, W. Yu, Y. J. Uemura, T. Klimczuk, J. D. Thompson, R. J. Cava, and G. M. Luke, Phys. Rev. B **82**, 024520 (2010).

[51] I. Bonalde, R. L. Ribeiro, W. Bramer-Escamilla, G. Mu, and H. H. Wen, Phys. Rev. B **79**, 052506 (2009).

[52] R. P. Singh *et al.*, A μSR study of non-centrosymmetric superconductor Zr_3Ir, STFC ISIS Neutron and Muon Source, https://doi.org/10.5286/ISIS.E.RB1720004 (2017).